3-17-2008

A MEMS Light Modulator Based on Diffractive Nanohole Gratings

Jack L. Skinner
Montana Tech

A. Alec Talin

David A. Horsley

A MEMS Light Modulator Based on Diffractive Nanohole Gratings

Abstract
We present the design, fabrication, and testing of a microelectromechanical systems (MEMS) light modulator based on pixels patterned with periodic nanohole arrays. Flexure-suspended silicon pixels are patterned with a two dimensional array of 150 nm diameter nanoholes using nanoimprint lithography. A top glass plate assembled above the pixel array is used to provide a counter electrode for electrostatic actuation. The nanohole pattern is designed so that normally-incident light is coupled into an in-plane grating resonance, resulting in an optical stop-band at a desired wavelength. When the pixel is switched into contact with the top plate, the pixel becomes highly reflective. A 3:1 contrast ratio at the resonant wavelength is demonstrated for gratings patterned on bulk Si substrates. The switching time is 0.08 ms and the switching voltage is less than 15V.

Comments
Jack L. Skinner is an Assistant Professor in the General Engineering Department at Montana Tech of the University of Montana.

A MEMS light modulator based on diffractive nanohole gratings

Jack L. Skinner[1,2,3*], A. Alec Talin[1,4], and David A. Horsley[2,3]

[1]*Sandia National Laboratories, Livermore, CA 94551*
[2]*Berkeley Sensor and Actuator Center, Berkeley, CA 94720*
[3]*Department of Mechanical and Aeronautical Engineering, University of California, Davis, CA 95616*
[4]*Center for Integrated Nanotechnologies, Albuquerque, NM 87185*
**Corresponding author: jlskinn@sandia.gov*

Abstract: We present the design, fabrication, and testing of a microelectromechanical systems (MEMS) light modulator based on pixels patterned with periodic nanohole arrays. Flexure-suspended silicon pixels are patterned with a two dimensional array of 150 nm diameter nanoholes using nanoimprint lithography. A top glass plate assembled above the pixel array is used to provide a counter electrode for electrostatic actuation. The nanohole pattern is designed so that normally-incident light is coupled into an in-plane grating resonance, resulting in an optical stop-band at a desired wavelength. When the pixel is switched into contact with the top plate, the pixel becomes highly reflective. A 3:1 contrast ratio at the resonant wavelength is demonstrated for gratings patterned on bulk Si substrates. The switching time is 0.08 ms and the switching voltage is less than 15V.

OCIS codes: (050.1950) Diffraction gratings; (050.6624) Subwavelength structures; (160.3918) Metamaterials; (160.4236) Nanomaterials; (230.4110) Modulators; (230.7408) Wavelength filtering devices; (240.6680) Surface plasmons; (240.6690) Surface waves.

References and links

1. J. B. Sampsell, "Digital micromirror device and its application to projection displays," J. Vac. Sci. Technol. B **12**, 3242-3246 (1994).
2. M. W. Miles, "MEMS-based interferometric modulator for display applications," Proc. SPIE **3876**, 20-28 (1999).
3. S. D. Senturia, D. R. Day, M. A. Butler, and M. C. Smith, "Programmable diffraction gratings and their uses in displays, spectroscopy, and communications," J. Microlithogr., Microfabr., Microsyst. **4**, 041401-041406 (2005).
4. I. W. Jung, J. S. Wang, and O. Solgaard, "Optical pattern generation using a, spatial light modulator for maskless lithography," IEEE J. Sel. Top. Quantum Electron. **13**, 147-154 (2007).
5. D. Rosenblatt, A. Sharon, and A. A. Friesem, "Resonant grating waveguide structures," IEEE J. Quantum Electron. **33**, 2038-2059 (1997).
6. Y. Kanamori, M. Shimono, and K. Hane, "Fabrication of transmission color filters using silicon subwavelength gratings on quartz substrates," IEEE Photon. Technol. Lett. **18**, 2126-2128 (2006).
7. W. Suh, O. Solgaard, and S. Fan, "Displacement sensing using evanescent tunneling between guided resonances in photonic crystal slabs," J. Appl. Phys. **98**, 033102 (2005).
8. Y. Kanamori, T. Kitani, and K. Hane, "Control of guided resonance in a photonic crystal slab using microelectromechanical actuators," Appl. Phys. Lett. **90**, 031911 (2007).
9. S. Y. Chou, P. R. Krauss, W. Zhang, L. Guo, and L. Zhuang, "Sub-10 nm imprint lithography and applications," J. Vac. Sci. Technol. B **15**, 2897 (1997).
10. R. W. Wood, "On a remarkable case of uneven distribution of light in a diffraction grating spectrum," Proc. Phys. Soc. London **18**, 269-275 (1902).
11. H. F. Ghaemi, T. Thio, D. E. Grupp, T. W. Ebbesen, and H. J. Lezec, "Surface plasmons enhance optical transmission through subwavelength holes," Phys. Rev. B **58**, 6779-6782 (1998).
12. K. L. van der Molen, F. B. Segerink, N. F. van Hulst, and L. Kuipers, "Influence of hole size on the extraordinary transmission through subwavelength hole arrays," Appl. Phys. Lett. **85**, 4316-4318 (2004).
13. J. M. Huang, K. M. Liew, C. H. Wong, S. Rajendran, M. J. Tan, and A. Q. Liu, "Mechanical design and optimization of capacitive micromachined switch," Sens. Actuators A **93**, 273-285 (2001).
14. C. Goldsmith, J. Ehmke, A. Malczewski, B. Pillans, S. Eshelman, Z. Yao, J. Brank, and M. Eberly, "Lifetime characterization of capacitive RF MEMS switches," IEEE MTT-S Int. Microwave Symp. Dig. **3**, 227-230 (2001).

#91642 - $15.00 USD Received 14 Jan 2008; revised 28 Feb 2008; accepted 1 Mar 2008; published 5 Mar 2008

15. W. M. Van Spengen, R. Puers, R. Mertens, and I. De Wolf, "A comprehensive model to predict the charging and reliability of capacitive RF MEMS switches," J. Micromech. Microeng. **14**, 514-521 (2004).
16. J. R. Reid, R. T. Webster, and L. A. Starman, "Noncontact measurement of charge induced voltage shift in capacitive MEM-switches," IEEE Microwave Wirel. Compon. Lett. **13**, 367-369 (2003).
17. P. G. Steeneken, T. G. S. M. Rijks, J. T. M. Van Beek, M. J. E. Ulenaers, J. De Coster, and R. Puers, "Dynamics and squeeze film gas damping of a capacitive RF MEMS switch," J. Micromech. Microeng. **15**, 176-184 (2005).
18. S. Chowdhury, M. Ahmadi, and W. C. Miller, "A closed-form model for the pull-in voltage of electrostatically actuated cantilever beams," J. Micromech. Microeng. **15**, 756-763 (2005).
19. J. B. Muldavin, "Design and analysis of series and shunt MEMS switches," Ph.D. dissertation, Dept. Elect. Eng. Comput. Sci., Univ. Michigan, Ann Arbor, MI (2001).
20. J. J. Blech, "On isothermal squeeze films," J. Lubr. Technol. **105**, 615-620 (1983).

1. Introduction

MEMS-based light modulators have broad applications in displays [1, 2], optical communication, spectroscopy [3], and maskless lithography [4]. In many of these applications (such as color displays and multicolor imagers), it is desirable for the modulator to have wavelength selective or wavelength-tunable characteristics. Many earlier wavelength selective elements have made use of optical interference generated by reflections from multiple thin film layers. In these devices, the peak reflectance (or transmittance) occurs at a wavelength (color) that is determined by film thickness. Realizing a multi-color pixel array with this approach poses the challenge that different film thicknesses must be deposited on each of the various pixel elements. A particular difficulty for MEMS devices (such as Fabry-Perot filters) exists in the difficulty to control the stress in a multilayer dielectric mirror, and as a result the optical surfaces of these MEMS devices are rarely flat. Here we describe an alternative approach based on interference between surface waves diffracted by a periodic array of subwavelength holes patterned into a metal film. Relative to devices based on multilayer dielectric mirrors, our approach has the advantage that it requires only a single thin-film metal layer, simplifying fabrication and stress control. In addition, since the reflectance spectrum is controlled by in-plane lithographic patterning, multicolor pixel arrays are readily realized with our approach.

A variety of filters and light modulators based on in-plane guided optical resonances have been demonstrated in recent years. Guided-mode resonant grating (GMRG) devices were used as optical band-stop filters at telecommunications wavelengths [5] and as visible color filters [6]. Similarly, the use of MEMS actuators to control guided resonances in photonic crystal slabs has been studied analytically [7] and was recently demonstrated at 1550 nm [8]. One challenge posed in fabricating these devices is the need for precise lithography with dimensional tolerances on the order of ~10 nm. Previous researchers have used electron beam or focused ion beam (FIB) lithography, but these techniques are ill-suited to fabricate large arrays of pixels (e.g. for imaging and display applications). We demonstrate pixels fabricated using low-cost nanoimprint lithography (NIL) [9], a technique capable of producing pixel arrays spanning an entire wafer.

2. Device operation

The device consists of an array of flexure-suspended silicon pixels bonded to a transparent glass plate. Similar to the glass used in liquid crystal display (LCD) applications, the glass plate is coated with a conductive indium tin oxide (ITO) layer and an insulating SiO_2 layer. The operation of a single MEMS pixel is illustrated schematically in Fig. 1. The front surface of each pixel is coated with a highly reflective metal (Ag or Al) patterned with a two dimensional array of subwavelength holes with diameter a and periodicity Λ [Fig. 1(a)]. As described below, the periodic pattern on the pixel surface results in a band-stop optical characteristic where the center wavelength (CWL) of the stop-band is approximately equal to $n\Lambda$, where n is the refractive index of the dielectric medium on the surface of the pixel. In the quiescent (OFF) state, an air gap separates the pixels from the surface of the glass plate [Fig. 1(b)]. A voltage applied between the ITO layer and the metal surface of the pixel results in an electrostatic force that causes the pixel to snap into contact with the glass plate, switching the

#91642 - $15.00 USD Received 14 Jan 2008; revised 28 Feb 2008; accepted 1 Mar 2008; published 5 Mar 2008

pixel into the ON state [Fig. 1(c)]. When the pixel is switched from the OFF state to the ON state, the refractive index on the pixel surface switches from $n = 1$ to $n = 1.5$, shifting the stop-band CWL out of the visible band and altering the spectrum of the reflected light.

The ability of periodically-patterned gratings to diffract light into propagating modes is well-known. In addition, gratings exhibit a variety of resonant modes that occur when the angle of incidence and grating period are chosen such that a propagating mode becomes evanescent. As a result, resonances are particularly evident in gratings whose period is close to (or smaller than) the operating wavelength, as such a grating may not support any propagating diffraction orders. Instead, the incident light is coupled into in-plane guided resonances. Metallic gratings exhibit both classical resonances, such as Wood's anomalies [10], and the more recently discovered resonances involving the coupling of light into surface plasmons (SPs) [11].

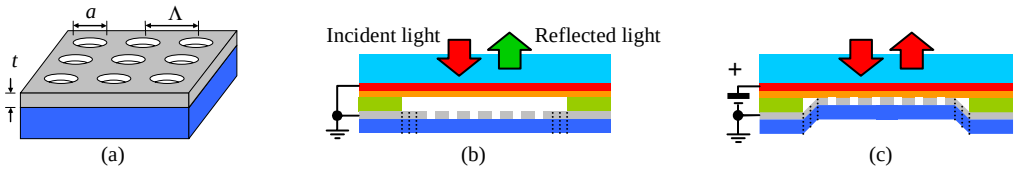

Fig. 1. (a). The pixel surface is coated with a metal of thickness t and patterned with a 2D square array of holes with period Λ and hole diameter a. (b) In the quiescent (OFF) state, no voltage is applied to the pixel; and an air gap separates the pixel from the glass plate. (c) The pixel is switched ON by applying a voltage between the ITO and metal layers, causing the pixel to snap into contact with the glass plate.

At normal incidence on a 2D square lattice, the Wood's anomalies [10] occur at wavelengths given by

$$\lambda_{ij} = n\Lambda \Big/ \sqrt{i^2 + j^2}\ . \tag{1}$$

where n is the refractive index, Λ is the grating periodicity, and i and j are integers representing the diffraction order. The SP-mediated resonances [11] occur at wavelengths close to the Wood's anomalies, as shown by

$$\lambda_{SP,ij} = \lambda_{ij} \sqrt{\varepsilon_m / \left(\varepsilon_m + n^2\right)}. \tag{2}$$

where ε_m represents the complex permittivity of the metal film. In our device, with $\Lambda = 500$ nm and a silver coating ($\varepsilon_m = -13.98 + 0.625i$), we expect the first resonances to occur at $\lambda_{01} = 500$ nm and $\lambda_{SP,01} = 519$ nm in the OFF state ($n = 1$), shifting to $\lambda_{01} = 727$ nm and $\lambda_{SP,01} = 789$ nm in the ON state ($n = 1.454$). Although the approximate CWL of each resonance can be calculated with Eq. (1) and Eq. (2), they do not incorporate the effect of hole diameter and film thickness, both of which are known to impact the CWL. To predict the exact CWL, depth, and spectral width of each resonance, we performed simulations using a commercial software implementation of rigorous coupled-wave (RCW) analysis (GD-Calc, KJ Innovation Software). The simulated reflectance, illustrated in Fig. 2, shows a deep notch at $\lambda = 550$ nm when the pixel is in the OFF state; whereas in the ON state, the pixel appears to be highly reflective over the entire 500 nm to 800 nm wavelength range. It should be noted that Eq. (1) and Eq. (2) consistently predict resonances at wavelengths shorter than those gathered from RCW modeling and experimental results. While the hole size of 170 nm was not strictly optimized, it was chosen as a reasonable compromise between resonance magnitude and width; the magnitude and bandwidth of the optical resonance is known to increase with increasing hole diameter [12].

#91642 - $15.00 USD Received 14 Jan 2008; revised 28 Feb 2008; accepted 1 Mar 2008; published 5 Mar 2008

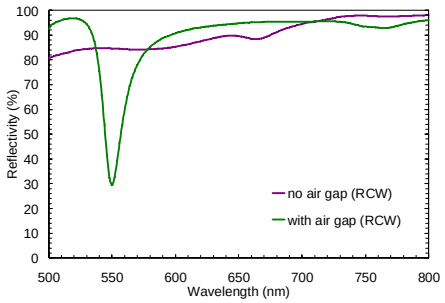

Fig. 2. Reflectivity of a silver-coated pixel with Λ = 500 nm, a = 170 nm, and t = 100 nm simulated using RCW analysis.

3. MEMS design

The MEMS pixel was designed so that a high quality nanohole grating could be fabricated on a flexure-suspended MEMS device. Figure 3 shows a schematic and a cross-section view of the pixel layout. Each 140 µm square pixel is suspended by four flexures with connections at the corners of the pixel. A photoresist (PR) layer separates the pixel array from the top glass plate. A voltage applied between the pixel and the top ITO electrode causes an electrostatic force, displacing the pixel upwards and decreasing the air gap. When the electrostatic force causes the pixel to deflect approximately one-third of the initial air gap, the pixel is pulled into contact with the SiO_2 layer on the top plate [13], switching into the ON state. The voltage at which switching occurs is referred to as the pull-in voltage, V_P. In the ON state, only a thin SiO_2 layer separates the ITO and pixel electrodes, greatly increasing the electrostatic force. As a result, a lower voltage, referred to as the hold voltage V_H, is sufficient to hold the pixel in the ON state after switching. This property allows a lower voltage to be used to maintain the ON state, an important attribute for low-power applications such as portable displays.

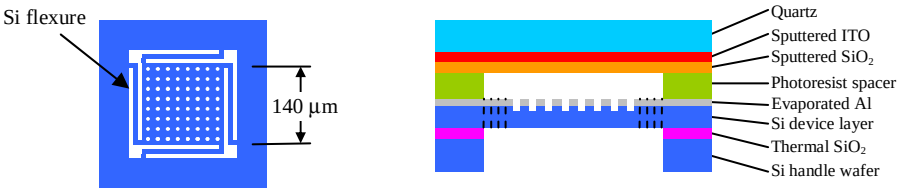

Fig. 3. (Left) Schematic representation of a single MEMS pixel supported by four flexures. The scale of the grating is exaggerated for clarity. (Right) Cross-section view showing the pixel chip bonded to a top glass plate coated with an indium tin oxide (ITO) top electrode and SiO_2 insulator.

4. Fabrication

The device fabrication process is illustrated in Fig. 4. A combined process involving nanoimprint lithography and contact lithography was used to pattern the nanohole grating and suspended MEMS structure, respectively. Completed pixels were then assembled onto a glass plate with photoresist used as a spacer layer.

#91642 - $15.00 USD Received 14 Jan 2008; revised 28 Feb 2008; accepted 1 Mar 2008; published 5 Mar 2008

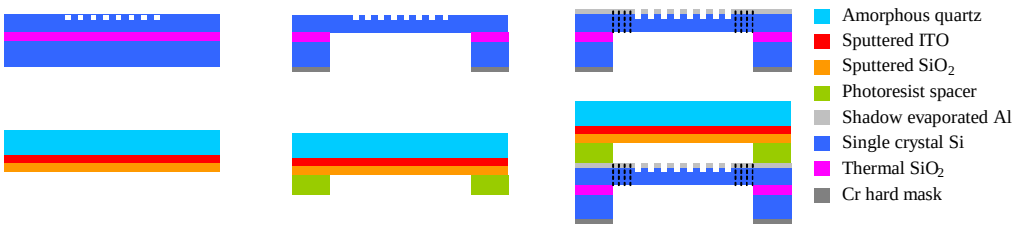

Fig. 4. Fabrication process flow for MEMS pixel arrays. Nanoimprint lithography (NIL) was used to pattern an array of nanoholes into the Si device layer. Contact lithography was used to pattern through wafer etch holes and the MEMS pixel structure. The top plate was made by depositing ITO and SiO_2 on a quartz wafer with patterned photoresist to provide the spacing between the pixel array and the top electrode.

Pixel arrays were fabricated using 100 mm silicon on insulator (SOI) substrates with a 2 μm thick Si device layer bonded to a 2 μm thick buried SiO_2 layer on a 500 μm thick Si handle wafer. First, the nanohole grating was patterned on the silicon device layer: NIL was used to pattern a 350 nm thick layer of polymethyl methacrylate (PMMA), after which this pattern was transferred to the Si device layer with a Cl_2/HBr plasma etch. Next, the MEMS pixel arrays were defined using two optical lithography and SF_6/C_4F_8 deep reactive ion etching (DRIE) steps. In the first step, the handle wafer Si and buried SiO_2 was removed beneath each pixel array to facilitate release of the pixels. A Cr hard mask was deposited and patterned on the backside of the wafer. DRIE was used to etch through the 500 μm thick Si handle layer, after which the buried SiO_2 was removed with by plasma etching. In the second step, the pixels and flexure suspensions were defined in the device Si through DRIE. A 60 nm thick layer of Al was deposited on the Si device layer through shadow evaporation with the wafer at 45 degrees to the Al source while rotating the wafer at 20 RPM. This process ensured that Al was deposited on the top surface of the Si device layer with no metal deposition in the bottom of the holes. Some amount of sidewall deposition occurs with shadow evaporation. The resulting tubular metallic structures have been observed by the authors to disrupt the resonant surface waves on the bottom side of the metal film. Resonance on both sides of the metal film is required for transmission enhancement, therefore limiting the use of such a technique primarily to reflective applications.

The top plate was fabricated from a fused quartz wafer sputtered with a 100 nm thick ITO film followed by a 330 nm SiO_2 film. The wafer was then spin coated with a 2 μm thick layer of photoresist (Shipley 1813) which was subsequently patterned to provide spacers to define the air gap between the pixel arrays and the top electrode. A completed MEMS pixel is shown in Fig. 5 along with the nanohole grating etched into the Si device layer. The MEMS pixel is 140 μm by 140 μm square with 10 μm wide flexures. The nanohole grating shows 140 nm wide holes etched about 250 nm deep with an array periodicity of 500 nm.

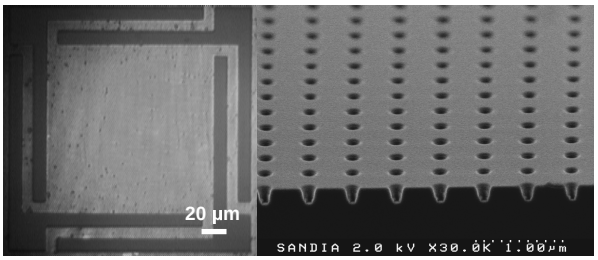

Fig. 5. (Left) Optical micrograph of completed MEMS pixel. The pixel is 140 μm by 140 μm square with 10 μm wide flexures. The nanohole pattern is not visible in the optical image. (Right) Scanning electron micrograph (SEM) of grating pattern etched into a silicon substrate by RIE.

#91642 - $15.00 USD Received 14 Jan 2008; revised 28 Feb 2008; accepted 1 Mar 2008; published 5 Mar 2008

Pixel curvature, due to stress in the grating metallization or buried SiO_2 layer, must be minimized to ensure proper optical performance. The pixel suspension was designed so that any initial curvature in the SOI wafer would result in rotation of the pixel flexures while leaving the pixel surface flat. Curvature was measured with a Veeco interferometric profilometer, as shown in Fig. 6. The radius of curvature for the X and Y profiles is 36.8 mm and 38.6 mm, respectively, for an average radius of curvature of 37.7 mm. A peak-to-valley deformation of 50 nm was observed across the pixel, corresponding to a wavefront accuracy better than $\lambda/10$ at the operating wavelength of 550 nm. Even higher flatness should be possible by employing a slightly thicker device Si layer and a thinner buried SiO_2 layer.

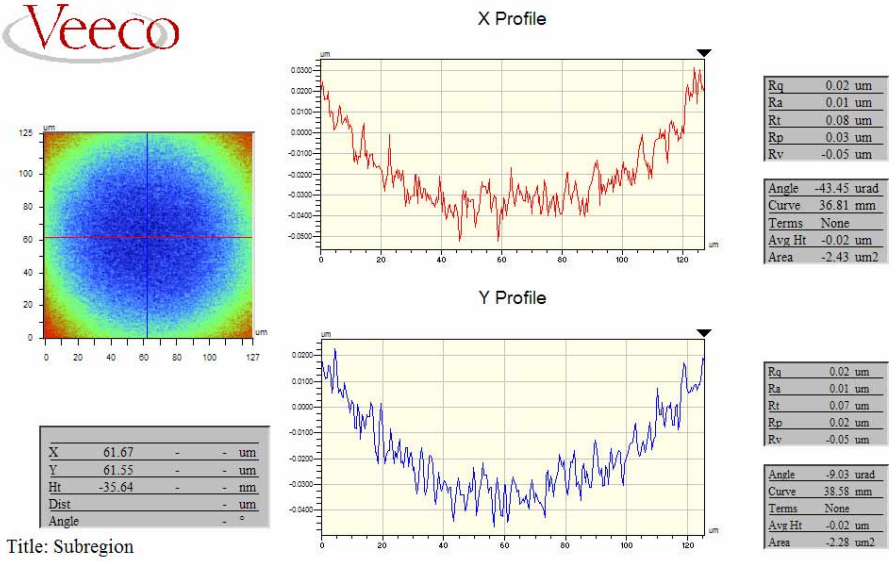

Fig. 6. Interferometric profile of MEMS pixel. The average measured radius of curvature of the pixel was 37.7 mm. The image is of the backside of the pixel, as the curvature of the pixel could not be measured through the top glass plate.

4. Experimental testing

Reflectivity measurements were collected with the use of a spectrometer coupled to an optical microscope. A tungsten filament lamp is used to provide a broadband source of light in the visible range. Light is directed through a beam splitter and a microscope objective. Light reflects from the grating and is collected by the objective and measured with a fiber coupled spectrometer (Ocean Optics USB2000). A computer is used to record the reflectivity spectrum. Reflectance measurements were performed using a 2x objective with a numerical aperture (NA) of 0.055. With the NA = 0.055, the half-angle of the illumination cone is 3.6°, ensuring both that the incident light is nearly collimated and that only the zero-order reflectance is collected.

Displacement measurements are done with the use of a laser Doppler vibrometer (LDV, Polytec OFV-3001). The LDV is used to measure the displacement at the center of each MEMS pixel. An electrostatic drive voltage is applied to between the MEMS pixel and the ITO electrode on the top glass wafer. Continuity between the Si device layer and Si handle layer is ensured by evaporating a layer of Al on the Si handle side of the wafer in the same process as used for fabricating the Al nanohole grating.

#91642 - $15.00 USD Received 14 Jan 2008; revised 28 Feb 2008; accepted 1 Mar 2008; published 5 Mar 2008

5. Results

5.1. Optical measurements

Optical observations of light reflected from a pixel in the ON and OFF state were made using a CCD camera coupled to a light microscope. Optical images of the pixel are shown in Fig. 7. The pixel was illuminated with filtered light spanning the wavelength range from 470 nm to 670 nm. The reflected light is seen to change from green-yellow in the OFF state to red in the ON state. Images of a pixel which do not have a nanoimprinted grating (only a smooth Al film) on its surface show almost no observable change in color.

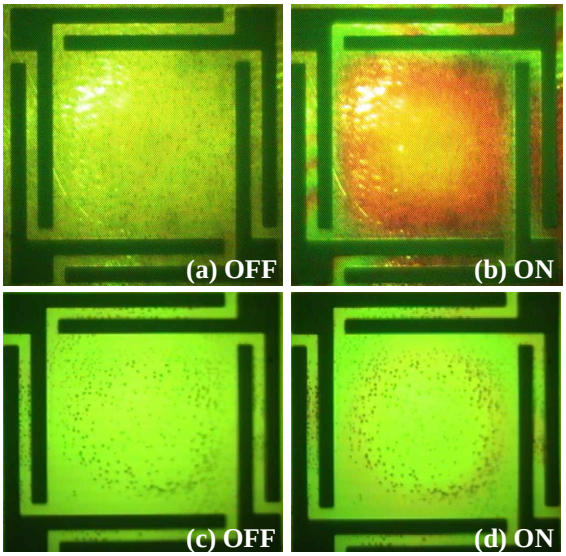

Fig. 7. Image of MEMS pixels when illuminated with green-yellow light and seen through a microscope. (a) and (b) show a pixel with a nanoimprinted Al grating, while (c) and (d) show a pixel that does not have the grating. (a) Pixel in the OFF state. (b) Actuated pixel in the ON state. Notice the change in color from green-yellow to orange-red with actuation. (c) Pixel in the OFF state. (d) Pixel in the ON state. (931 KB) Movie of light modulation with MEMS pixel with grating. (880 KB) Movie showing a pixel without the nanoimprinted grating switching ON and OFF.

To improve the signal-to-noise ratio for quantitative reflectivity measurements, large area (25 mm x 25 mm) nanohole gratings were prepared on Si substrates using the same NIL template used for MEMS pixel fabrication. Gratings were coated with Al and Ag layers to allow comparison of the effect of different metals on the reflectance spectrum. For each grating, two reflectance measurements were performed: the first with the grating in contact with a fused silica plate and the second with a small ~10 μm air gap between the two surfaces. The results of these measurements are presented in Fig. 8. The higher conductivity of the Ag grating results in a deeper optical stop-band with a narrower spectral width than the Al grating. The measured Ag grating spectra show good agreement with the simulated spectra shown in Fig. 2 produced using RCW analysis. While not explicitly shown here, similar agreement between measured spectra and RCW analysis can be expected with Al, or any metal where the complex optical properties are known. In addition, the CWL of the Ag grating is approximately 1.5 % longer than the CWL of the Al grating (558 nm versus 550 nm). This difference may be due to the difference in permittivity of the two metals – given the same grating dimensions, the SP model from Eq. (2) predicts that a Ag grating will have a 2 % longer CWL than an Al grating. Although the agreement between the SP model and the measured data seems promising, it is also possible that the difference in CWL is caused by

#91642 - $15.00 USD Received 14 Jan 2008; revised 28 Feb 2008; accepted 1 Mar 2008; published 5 Mar 2008

other effects, such as differences in the surface roughness or final nanohole diameter in the two gratings. The reflectivity of the Ag grating is 29.3 % at λ = 558 nm in the OFF state and increases to 90 % in the ON state, corresponding to contrast ratio of approximately 3:1. In comparison, the Al grating reflectivity is 50 % at λ = 550 nm in the OFF state, increasing to 92.5 % in the ON state, a contrast ratio of 1.9:1. Reflectivity was measured up to a maximum wavelength of 900 nm on the Ag grating, confirming that switching from the OFF state to the ON state shifts the CWL of the grating resonance from 558 nm to 879 nm (a factor of 1.58), in good agreement with the expected shift predicted based on the refractive index of fused silica (n = 1.54 at λ = 879 nm).

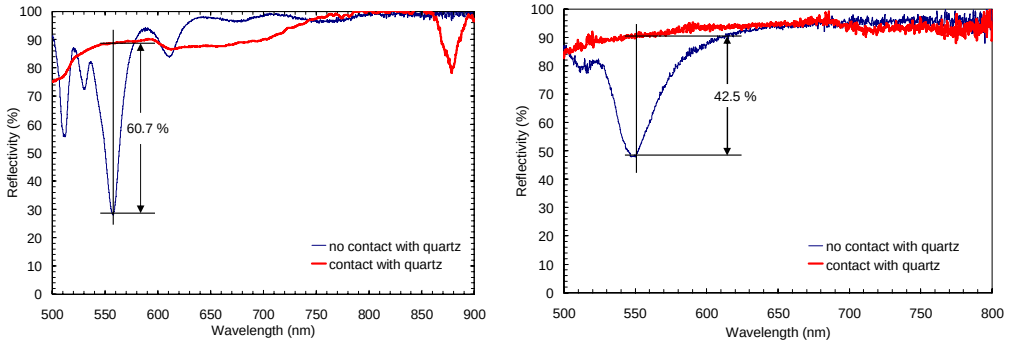

Fig. 8. Reflectivity measurements performed on large area gratings. Each grating was mounted beneath a glass wafer, and the reflectivity was measured with the grating pressed into contact with the glass wafer and separated by an air gap. Left: Ag grating. Right: Al grating.

Reflectivity spectra of Al coated MEMS pixels in the ON and OFF states were measured using an aperture to limit the field of view to a 4 x 4 array of pixels. The pixel spacing and flexure suspension geometry are such that the active pixel surface had a fill-factor of approximately 65 % in this measurement. The measured reflectivity spectra, shown in Fig. 9, demonstrate a reflectivity of 34 % at 560 nm in the OFF state and a reflectivity of 55 % in the ON state, a contrast ratio of ~1.6:1. The measured contrast ratio of the MEMS array is considerably lower than that measured on the bulk gratings due to the relatively low fill-factor in the prototype device. The OFF state reflectivity of the pixel array is similar to that of the bulk Al grating. However, the ON state reflectivity is considerably lower than the 90 % achieved in a bulk grating device, since only the pixel surface is actively modulated in and out of contact with the top plate. As illustrated in the figure, when the pixel is switched from the OFF state to the ON state, the reflectivity is reduced in the 490 nm to 540 nm (green) wavelength range and increases in the 540 nm to 650 nm (yellow-orange) wavelength range, in qualitative agreement with the optical images shown in Fig. 7. A subtractive color model, such as CMYK (cyan, magenta, yellow, and key), is applicable to color reproduction for the shown MEMS pixel made with a metal film perforated with holes. The complementary structure with an array of isolated metal dots would be more amenable to an additive color model, such as RGB (red, green, and blue), which is a standard color model used for color displays. A quantitative description of the reproducible color gamut is difficult to provide; however, the presented MEMS pixel shows promise for a color gamut comparable to LCD (liquid crystal display) technology.

No long term reliability tests were performed on the MEMS pixel. However, the devices tested were designed so that the yield strength of the Si flexures was not exceeded. This eliminated the possibility of first cycle failure. As long as such a device is designed properly, mechanical failure should not be the life-limiting factor. Optical characteristics of the grating are expected to remain stable over time, but this has yet to be verified through long-term testing. The primary mode of failure of the MEMS pixel is expected to be charging of the electrical insulating SiO2 layer, similar to the primary mode of failure of capacitive radio

#91642 - $15.00 USD Received 14 Jan 2008; revised 28 Feb 2008; accepted 1 Mar 2008; published 5 Mar 2008

frequency (RF) MEMS switches [14]. Effects of charging on device lifetime is fairly well understood [15] and should be addressed during the design phase of any such capacitive device.

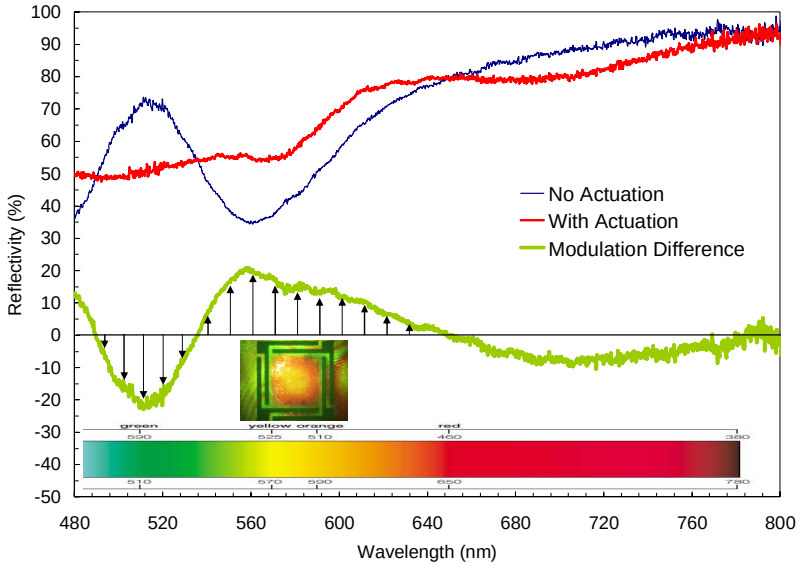

Fig. 9. Reflectivity measurements of a MEMS pixel with and without actuation. The reflectivity at 560 nm is 34 % in the OFF state and 55 % in the ON state.

5.2. Switching measurements

The pull-in voltage V_P and hold-down voltage V_H were measured by actuating a pixel with a 15V triangular drive voltage and recording the pixel displacement using the LDV. The voltage dependent displacement is shown in Fig. 10. The time history of the displacement data is indicated on the plot with arrows showing the pixel motion as the voltage is first increased from 0 V to +15 V, then decreased from +15 V to -15 V before finally returning to 0 V. The fact that the measurement is not symmetric about 0 V suggests that charge has accumulated in the SiO_2 dielectric on the top plate [16, 17]. We estimate the trapped charge on the SiO_2 surface [17] as $\sigma = 25$ nC/cm^2 using $\sigma = \Delta V \varepsilon_r \varepsilon_0 / t_d$, where $\Delta V = 2.4$ V is the offset in the line of symmetry, $\varepsilon_0 = 8.85$ pF/m is the permittivity of vacuum, and $\varepsilon_r = 3.9$ and $t_d = 330$ nm are the dielectric constant and thickness of the SiO_2 dielectric layer, respectively.

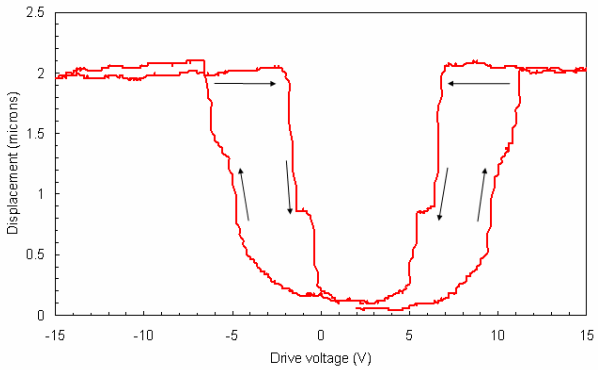

Fig. 10. Measured pixel displacement versus applied voltage. The arrows indicate the direction of pixel motion as the voltage is swept from 0 V to 15 V, back down from 15 V to -15 V, then returning from -15 V to 0 V.

#91642 - $15.00 USD Received 14 Jan 2008; revised 28 Feb 2008; accepted 1 Mar 2008; published 5 Mar 2008

An analytical expression for the pull-in voltage V_P [18] is given by

$$V_P = \sqrt{8k\left(g + t_d/\varepsilon_r\right)^3/\left(27\varepsilon_0 A\right)} \tag{3}$$

where k = 6.0 N/m denotes the stiffness of the mechanical suspension, g = 2 μm is the initial air gap, and A = 140 x 140 μm^2 is the area of the pixel. Given these design parameters, the pull-in voltage predicted using Eq. (3) is V_P = 9.6 V. Correcting for the 2.4V offset discussed above, the measured pull-in voltage is 8.8V, in good agreement with the analytical model.

Similarly, the hold voltage V_H [19] can be predicted using

$$V_H = \sqrt{27}t_d V_P/\left(2g\varepsilon_r\right). \tag{4}$$

The predicted hold voltage is V_H = 1.1 V, whereas the offset-corrected hold voltage was measured to be 3.6V. We believe the discrepancy between the measurement and the analytical model may be due to the fact that the flexures create a slight curvature in the pixel surface when the pixel is in the ON state. This curvature results in a slight air gap at the edges of the pixel [visible as a color variation at the edges of the pixel in Fig. 7(b)], reducing the electrostatic force available to hold the pixel down.

The measured time-dependent pixel displacement in response to a 23V step input is shown in Fig. 11. The measured switching time is t_s = 80 μs.

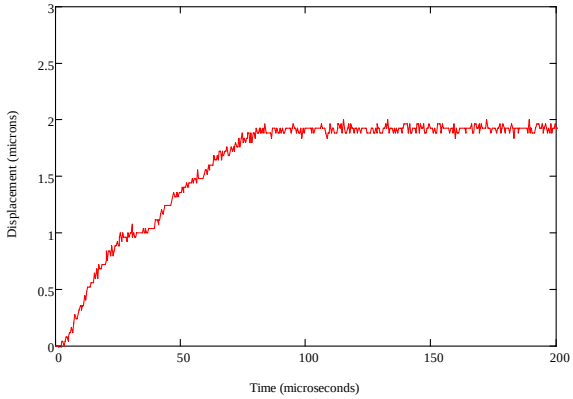

Fig. 11. Measured deflection of MEMS pixel from application of 23 V square wave. Switching time is 80 μs.

The switching time has a complicated relationship with the electromechanical properties of the MEMS device due to the fact that the pixel is subjected to electrostatic force and squeeze-film gas damping, both of which vary nonlinearly with the air gap. At a given air gap g the squeeze-film damping coefficient is expressed as [20]

$$b = \left(3/2\pi\right)\mu A^2/g^3 \tag{5}$$

where μ = 1.845·10^{-5} Pa·s is the viscosity of air at standard temperature and pressure (STP). When a step voltage $V_S > V_P$ is applied to the pixel, a closed form approximation for the switching time t_s can be derived by neglecting the pixel inertia and suspension stiffness and replacing the squeeze-film damping with a gap-independent viscous damping model. Under these conditions, the switching time is given by

$$t_s = 2bg_0^3/\left(3\varepsilon_0 A V_S^2\right) \tag{6}$$

where b denotes the damping coefficient, g_0 is the initial air gap, and V_S is the amplitude of the step voltage. The damping constant predicted using Eq. (5) varies from 0.4 mN·s/m to 3.4 mN·s/m as g varies from 2 μm to 1 μm. Using b = 1.4 mN·s/m and V_S = 23 V in Eq. (6)

#91642 - $15.00 USD Received 14 Jan 2008; revised 28 Feb 2008; accepted 1 Mar 2008; published 5 Mar 2008

gives t_s = 80 μs. For reference, the switching time of a liquid crystal device is typically an order of magnitude slower. Although the amplitude of V_S contributes to the fast switching time, Eq. (6) suggests that reducing V_S by a factor of two would only increase the switching time to ~0.3 ms.

7. Conclusion

MEMS pixel arrays based on resonant gratings have the potential for unique optical characteristics. Since the resonant wavelengths are defined through lithography, considerable flexibility is available for the design of multicolor pixel arrays. Although grating fabrication requires precise nanolithography, NIL is low cost and suitable for fabricating wafer-scale (or larger) pixel arrays. Measured optical performance of the pixel arrays corresponds well to simulations produced using RCW analysis. The relatively low fill-factor of the first prototype devices could be greatly increased by reducing the space between pixels. With a fill factor closer to 100 %, the MEMS pixel array should achieve the 3:1 modulation contrast ratio measured on bulk grating devices. Optimization of the grating design through RCW studies is likely to result in further increases in contrast ratio. The measured switching time and switching voltage agree well with the predictions of analytical models. Although the switching voltage is relatively low for an electrostatic MEMS device, it is still somewhat higher than desired for many portable display devices. The fact that the switching time is much faster than required for these applications suggests that some design flexibility exists to optimize the MEMS design (e.g. to reduce the switching voltage at the cost of slower switching speeds).

Acknowledgments

We gratefully acknowledge the help of Professor S. J. Brueck and the Center for High Technology Materials at University of New Mexico for fabrication of the original nanoimprint template. Work performed by Sandia National Laboratories is under the auspices of the U.S. Department of Energy, Contract No. DEAC04-94AL85000.

#91642 - $15.00 USD Received 14 Jan 2008; revised 28 Feb 2008; accepted 1 Mar 2008; published 5 Mar 2008